

Helicity amplitudes for photoexcitation of nucleon resonances off neutrons

A.V. Anisovich^{1,2}, V. Burkert³, E. Klempt¹, V.A. Nikonov^{1,2}, A.V. Sarantsev^{1,2}, U. Thoma¹

¹ Helmholtz-Institut für Strahlen- und Kernphysik, Universität Bonn, Germany

² Petersburg Nuclear Physics Institute, Gatchina, Russia

³ Jefferson Lab, 12000 Jefferson Avenue, Newport News, Virginia, US

Received: July 14, 2018/ Revised version:

Abstract. The helicity amplitudes $A_n^{1/2}$ and $A_n^{3/2}$ for the photoexcitation of nucleon resonances off neutrons are determined in a multi-channel partial-wave analysis.

1 Introduction

One of the most intriguing issues in the physics of strong interactions is the spectrum and internal structure of baryon resonances [1,2,3]. In the calculation of mesonic excitations, quark models have been very successful [4,5]. Classical examples are the non-relativistic quark model [6] and its relativized [7] or fully relativistic versions [8,9]. These models use a linear confinement potential simulating confinement and some residual quark-antiquark interactions. But in the baryon sector, the situation is much more complicated. In the low mass region, the interpretation of baryons as three-quark bound states in a linear confinement potential appears to be rather successful, even though important details such as the masses of radial excitations like the Roper resonance $N(1440)1/2^+$ remain unexplained [10,11,12]. The choice of a different form of the confinement potential [13] or of the residual interaction [14] improves the mass pattern. More recently, dynamical approaches such as the dynamically coupled channel models [15], that include coupling to inelastic channels, have been successful in predicting the correct pole structure of this state. At higher masses quark models predict a large number of states which were not found experimentally up to now. This problem triggered two developments: the start of new experiments searching for these *missing resonances*, and elaboration of new theoretical models which can explain the observed spectrum.

The most direct approach to calculate the masses of baryon excitations is to discretize QCD on a lattice [16,17]. It turns out, however, that the number of states is identical to the number expected in a simple picture where the three-body system is described by two harmonic oscillators, at least in the first and second excitation band. In the low-energy region, the mass pattern resembles the ob-

served spectrum. At the present stage, lattice QCD computations still use unphysical quark masses, and do not include decays of excited states. They therefore provide no explanation why a large fraction of the states remains unobserved. Also, the predicted mass spectrum does not agree with observations.

Possibly, quarks are not the only degrees of freedom to describe baryon resonances, they may possibly be better described by the interaction of stable (or quasi-stable) hadrons, from the interaction of mesons and baryons. The interaction is then derived from chiral Lagrangians, from an effective theory of QCD at low energies [18,19,22,20,21]. Great progress has been made in a better understanding of the properties of a few baryon resonances. At present, it is however not yet clear what spectrum emerges in this approach, and it is even unclear if these dynamically generated states come atop of quark model states or if they reflect a better understanding of quark model states. Measurements of helicity amplitudes will be essential in trying to discern the internal structure of these states.

Up to recently, our experimental knowledge of the baryon spectrum was based mostly on the classical analyses [23,24] at Karlsruhe and Carnegie-Mellon and on the more recent analysis at GWU [25] of data on elastic πN scattering. The large inelasticity in all partial waves demonstrates the importance of inelastic reactions. Yet, pion-induced inelastic data have rather poor statistic and, sometimes, there are contradictions between different experiments. But there is a wealth on new data from photoproduction experiments [26]. A multichannel partial wave analysis of these data allowed us to confirm the existence of resonances which were ambiguously identified in the analysis of the elastic πN data, to observe new states, and to define many properties of baryons with a good precision [27]. The analysis hence yields important information on resonance couplings to different final states but also on

the γN channel. These couplings depend on the internal structure of baryons and can be calculated in the framework of different models. A list of the γp and γn couplings calculated in the framework of a relativized quark model can be found in [28]. The agreement between calculated and observed values is one of the remarkable successes of the quark model. Other models do not yet provide the full list of the γN couplings although for separate states such calculations can be found in the literature: see, for example, the calculation of the Roper γN couplings with the AdS/QCD approach [29]. There is no doubt that a relevant model should reproduce not only masses of baryons but also their decay properties.

Knowledge of the resonance photocouplings can give insight into the underlying symmetry and internal structure of the states. For example, the Single Quark Transition (SQT) model [30,31] describes the electromagnetic transitions from the ground state nucleon to all states within the $SU(6)$ multiplets $(70, 1^-)_1$ and $(56, 2^+)_2$ with just 3 and 4 reduced amplitudes, respectively. With accurate data on the photocoupling amplitudes for these states, these relationships can be tested and provide further insights into the underlying symmetry. Surprisingly good results were found for the $(70, 1^-)_1$ multiplet [32], for which the reduced amplitudes were determined from the well-measured $N(1535)1/2^-$ and $N(1520)3/2^-$ photocoupling amplitudes on protons, and used to predict the remaining 14 amplitudes for states in this multiplet on both protons and neutrons. Strong deviations from these predictions for individual states would indicate that contributions other than single quark transitions may contribute or that the assignment of the state to a specific (D, L_N^P) multiplet is questionable.

In this paper we report the result of the combined analysis of the data base used for solutions BG2011 [27] with data on π^- , π^0 , and η photoproduction off neutron. The data are not sufficiently precise to increase our knowledge of masses, widths and hadronic decay modes of baryon resonances. Hence all these quantities can remain frozen, and only the γn helicity couplings are free parameters of the fit. In a final fit all parameters are set free; this gives a slight improvement in χ^2 without significant changes in any of the parameters. The fit returns these helicity amplitudes. They are tabulated here and compared with previous determinations.

2 Data base

The data used for the determination of the γn couplings of the N^* states are listed in Table 1. In addition to the new JLab data on $\gamma n \rightarrow p\pi^-$ [35,36] a large number of further data on this reaction [37,38,39,40,41,42] has been included in the fit.

In bubble chambers all outgoing charged particles are detected [43,44] and the events are kinematically fully reconstructed. No correction for Fermi motion is hence required. We give the χ^2 contribution for the latter data separately. Several groups have reported measurements on the beam asymmetry Σ using linearly polarized photons

Table 1. Data base for meson production off neutrons as compiled by Data Analysis Center at GWU [77]. The table lists the reaction and reference to the original work, the observable, the number of data points, and two χ^2 values. χ_0^2 shows the quality of the fit using solution BG2011-02 with γn couplings as free parameters only. The χ_f^2 shows the quality of the fit to the γn data after optimization of all parameters.

$\gamma n \rightarrow \pi^- p$	Observ.	N_{data}	χ_0^2	χ_f^2
[36, 37, 38, 39, 40, 41, 42]	$d\sigma/d\Omega$	1298	2.84	2.32
[43, 44]	$d\sigma/d\Omega$	529	3.16	3.08
[45, 46, 47, 48, 49, 50, 51, 52, 53]	Σ	316	3.74	3.08
[54, 55, 56, 57]	T	105	4.96	3.18
[58, 59]	P	20	3.22	3.17
<hr/>				
$\pi^- p \rightarrow \gamma n$				
[60, 61, 62, 63, 64, 65, 66]	$d\sigma/d\Omega$	495	1.65	1.53
[67, 68]	P	55	4.59	3.11
<hr/>				
$\gamma d \rightarrow \pi^0 n(p)$				
[69, 70, 71, 72]	$d\sigma/d\Omega$	147	3.14	2.98
[73]	Σ	216	2.82	1.90
<hr/>				
$\gamma d \rightarrow \eta n(p)$				
[74]	$d\sigma/d\Omega$	330	1.57	1.40
[75]	Σ	88	2.42	2.17

[45,46,47,48,49,50,51,52,53] and the target asymmetry T using a transversely polarized deuteron target [54,55,56,57]. The recoil polarization of the proton P was determined by exploiting the analyzing power of the proton-Carbon scattering process [58,59].

The reverse reaction $\pi^- p \rightarrow n\gamma$ has the advantage that no Fermi correction needs to be applied. Data were taken at several laboratories [60,61,62,63,64,65,66]. By polarizing the target protons, the polarization variable P is determined [67,68].

Differential cross sections for photoproduction of neutral pions off neutrons $\gamma d \rightarrow n\pi^0(p)$ are obtained using a deuteron target [69,70,71,72]. The beam asymmetry Σ for this reaction is available from [73]. Similar data exist for $\gamma d \rightarrow \eta\gamma(p)$ [74,75].

Data obtained with a deuteron target are affected by the Fermi motion of the neutron and by rescattering in the final state (Final State Interaction, FSI). The results thus depend on the cuts made in the experiment or the analysis: for example, a particular cut on the momentum of the spectator proton influences the smearing of the data due to Fermi motion and the contribution from the FSI.

The treatment of the Fermi motion in our approach was described in detail in [33]. For the FSI we use the corrections calculated by the SAID group [36,76]. Here, we have restricted the fitted energy interval to invariant masses below 2.3 GeV since above, too little is known about photoproduction of resonances. The data on η photoproduction data off neutrons seem to suffer less from FSI. The $\gamma d \rightarrow \eta p(n)$ cross sections agree very well with data on $\gamma p \rightarrow \eta p$. Thus here we follow the prescription of

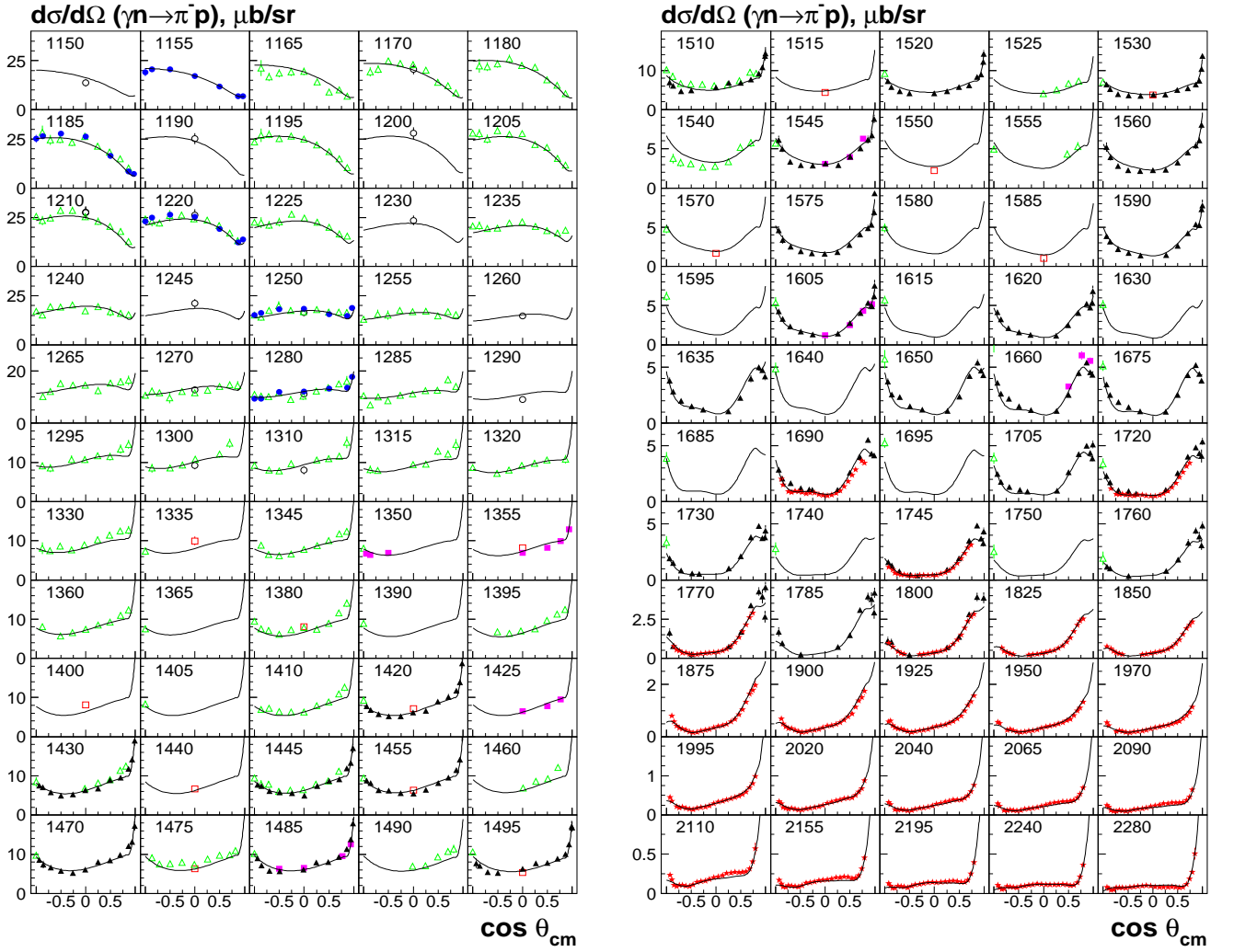


Fig. 1. Differential cross section for $\gamma n \rightarrow \pi^- p$. Data: red filled stars are from [36], black open circles are from [37], red open squares are from [38], green open triangles are from [39], blue filled circles are from [40], pink filled squares are from [41], black filled triangles are from [42].

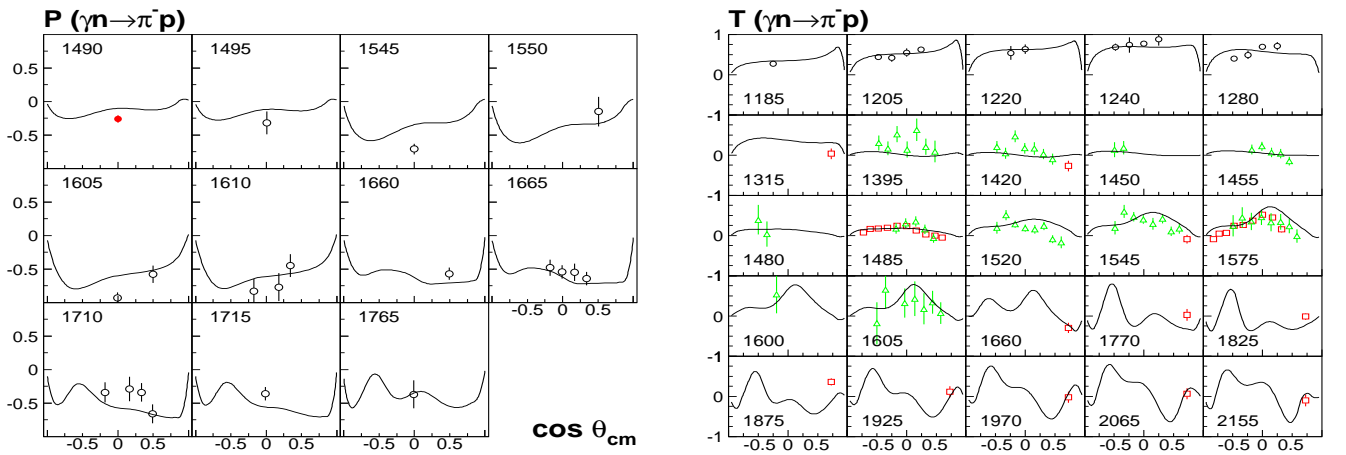


Fig. 2. Left: Recoil polarization P for $\gamma n \rightarrow \pi^- p$. Data: black open circles are from [58], red filled circles are from [59]. Right: Target polarization T of $\gamma n \rightarrow \pi^- p$ reaction. Data: black open circles are from [54], red open squares are from [55,56]. Green open triangles are from [57].

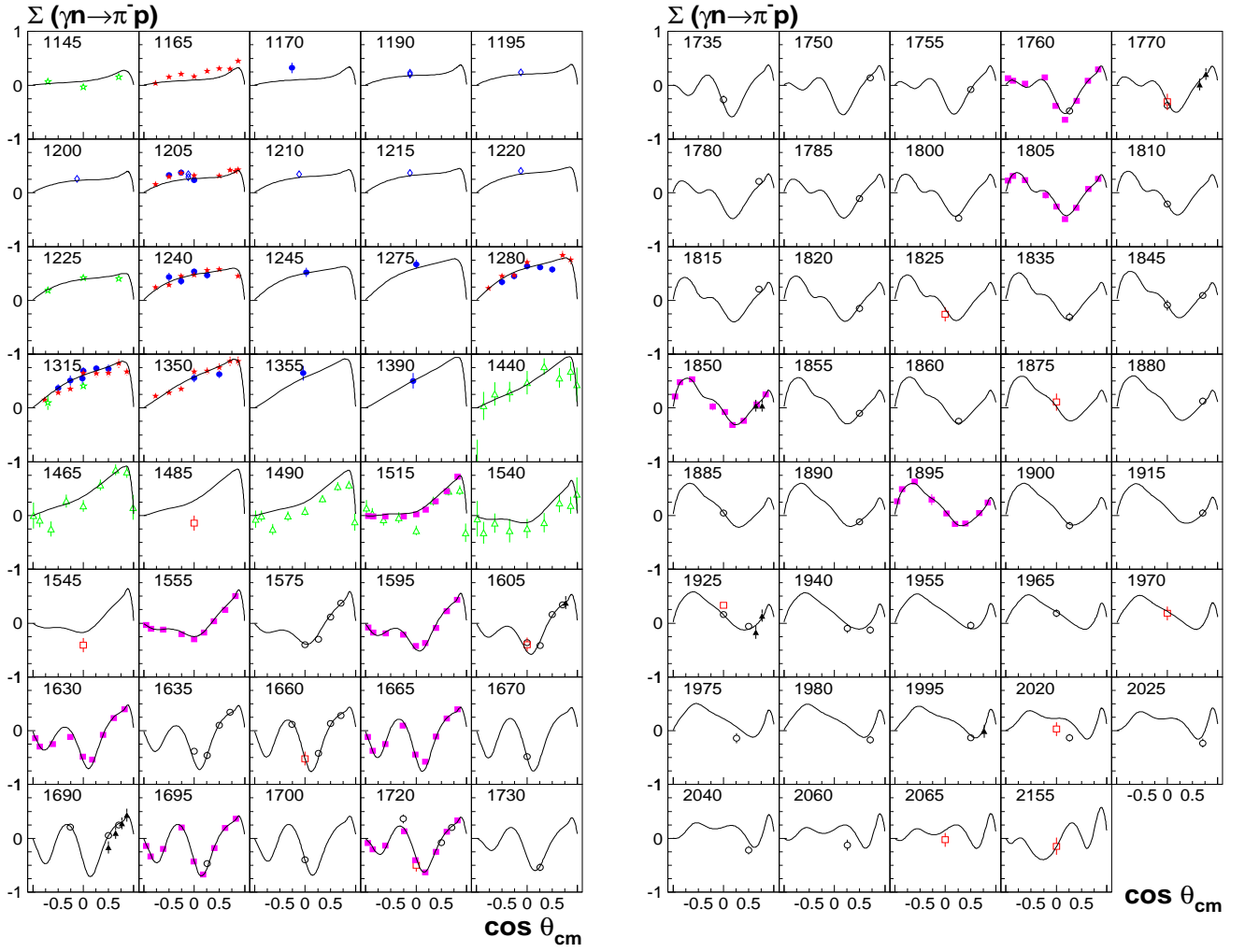


Fig. 3. Σ polarization for $\gamma n \rightarrow \pi^- p$. Data: black open circles are from [45], red open squares are from [46], green open triangles are from [47], blue filled circles are from [48], pink filled squares are from [49], black filled triangles are from [50], red filled stars are from [51], green open stars are from [52], blue open diamonds are from [53].

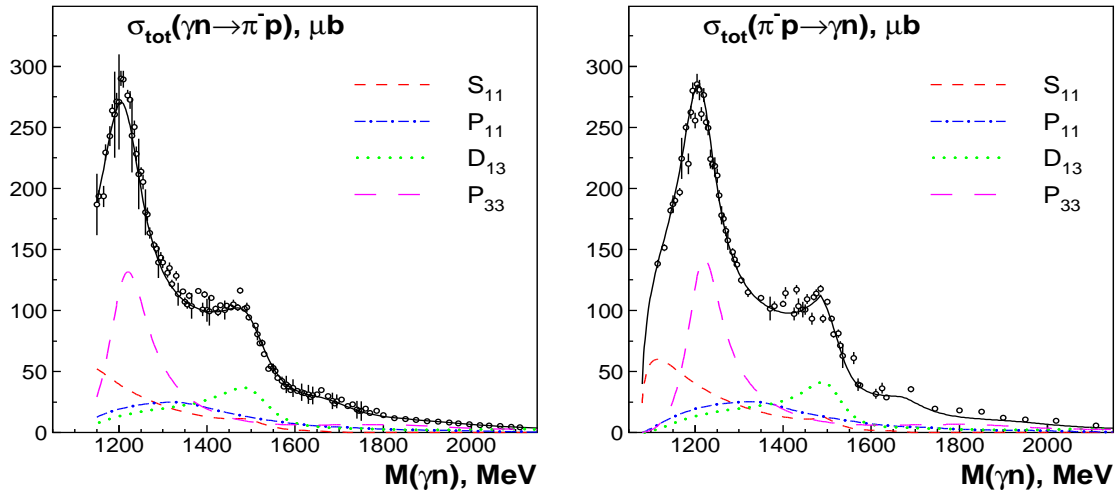


Fig. 4. Left: Total cross section for $\gamma n \rightarrow \pi^- p$. The Fermi motion is taken into account. Right: Total cross section from the $\pi^- p \rightarrow \gamma n$ reaction, and from data on $\gamma n \rightarrow \pi^- p$ reaction with full kinematics. Corrections for Fermi motion are not required.

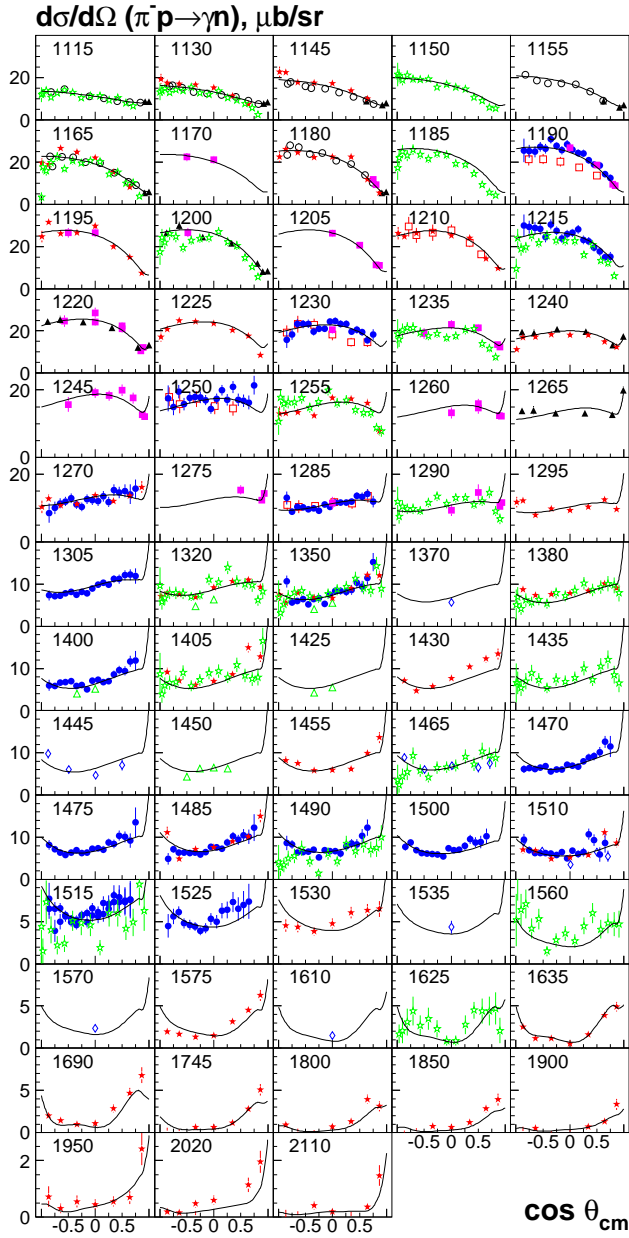


Fig. 5. Differential cross section for $\pi^-p \rightarrow \gamma n$. Data: black open circles are from [60], red open squares are from [61], green open triangles are from [62], blue filled circles are from [63], pink filled squares are from [64], black filled triangles are from [65], red filled stars are from [43], green open stars are from [44], blue open diamonds are from [66].

paper [74] where the difference between two approaches to allow for FSI was included as a systematic error.

3 Fits to the data

As the first step we fitted γn data starting from solutions BG2011-01 and BG2011-02, respectively. Due to the incompleteness of the data, several solutions exist which give

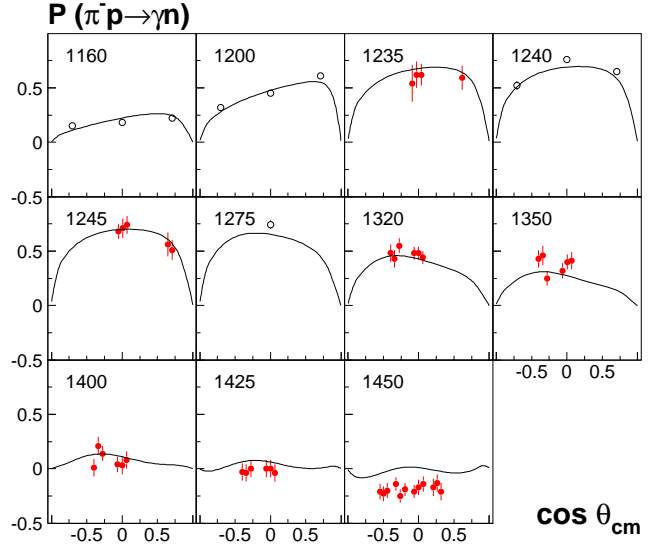


Fig. 6. Recoil polarization P for $\pi^-p \rightarrow n\gamma$. Data: black open circles are from [67], red filled circles are from [68].

a similar quality in the data description. The most significant differences were found in the $1/2(3/2^+)$ wave where BG2011-02 finds two close-by resonances: $N(1900)3/2^+$, present in both types of solutions with slightly different parameters, and $N(1975)3/2^+$, present only in BG2011-02. But also in the $1/2(5/2^+)$ wave, solutions exist with two or three poles, the well known $N(1680)5/2^+$ and a second resonance at about 2090 MeV or, alternatively, $N(1680)5/2^+$ and two resonances at about 1860 MeV and 2190 MeV.

The description of the data, obtained when starting from the solution BG2011-01 appeared to be systematically worse than that from the solution BG2011-02. Fig. 1 shows differential cross sections for $\gamma d \rightarrow p\pi^-(p)$ from JLab [36] and earlier measurements [37, 38, 39, 40, 41, 42]. The data on recoil polarization P and target asymmetry T are shown in Fig. 2, those on the beam asymmetry Σ in Fig. 3.

The data on $\gamma d \rightarrow p\pi^-(p)$ are fitted simultaneously with data on the inverse reaction $\pi^-p \rightarrow n\gamma$ [60, 61, 62, 63, 64, 65, 66, 67, 68] (and data from bubble chambers [43, 44]) which are free from Fermi corrections. The total cross sections for these two reactions - linked by time reversal invariance - are shown in Fig. 4. The data points represent the summation over the differential cross sections; uncovered angular regions are taken from the fit to the data presented in Figs. 1-3. The data on $d\sigma/d\Omega$ and on P from the inverse reaction $\pi^-p \rightarrow n\gamma$ are shown in Figs. 5 and 6, respectively.

Resonance contributions to the reaction $\gamma d \rightarrow n\pi^0(p)$ are related to $\gamma d \rightarrow p\pi^-(p)$ by Clebsch-Gordan coefficients. For the decay of Δ resonances, the $p\pi^-$ decay is disfavored by a factor 2 compared to $n\pi^0$, for nucleon resonances, this is reversed. At the production vertex, the situation is a bit more complicated. The isospin $3/2$ partial waves are produced with the same couplings in the γp and γn interaction which imposes particular relations on the t- and u-exchange amplitudes. In the case of pro-

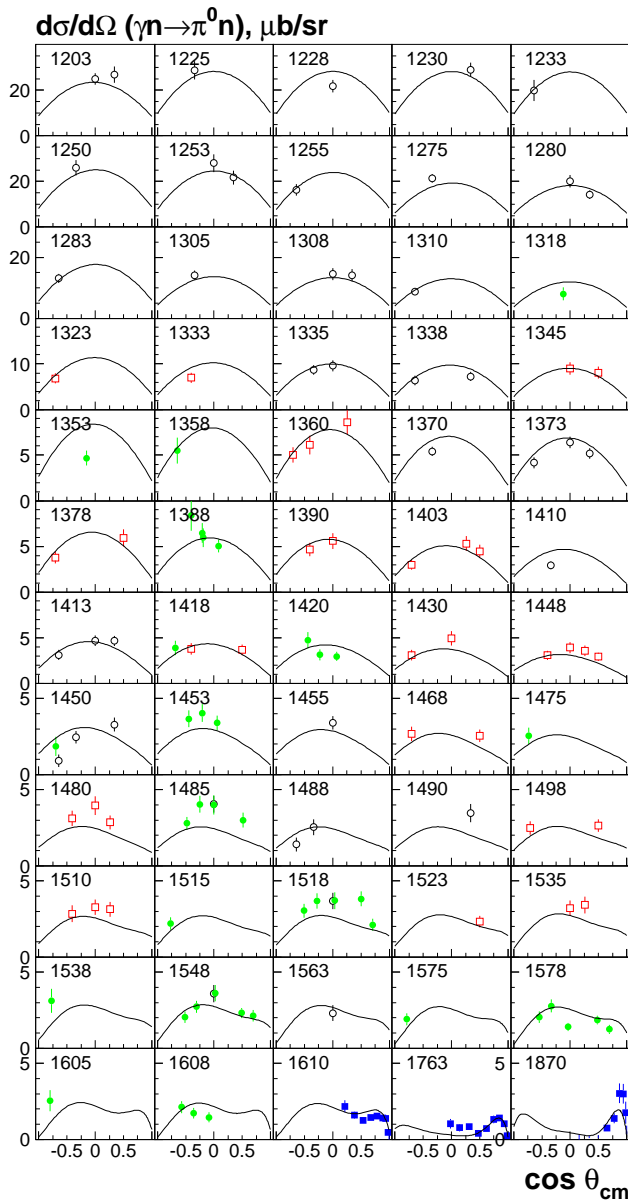


Fig. 7. Differential cross section for $\gamma n \rightarrow \pi^0 n$. Data: black open circles are from [69], red open squares are from [70], green filled circles are from [71], blue filled squares are from [72].

duction of neutral mesons the fitting of the γn and γp reactions helps to distinguish between (reggeized) t-channel exchanges with isospin 1 and 0, e.g. ρ and ω exchanges. In the case of photoproduction of charged pions off neutrons, the t-channel exchange is fully fixed from the fit to the reactions with γp in the initial state.

The $\gamma n \rightarrow \eta n$ differential cross section shows a peak in the mass region 1700 MeV which can be described either as an interference (including cusp-) effect in the $J^P = 1/2^-$ partial wave or as a contribution from a narrow state $N(1680)$ in the $J^P = 1/2^+$ partial wave. In the present analysis every fit was made with and without contribution from the $N(1680)$ state. All these solutions were included to define the systematic errors for the γn couplings.

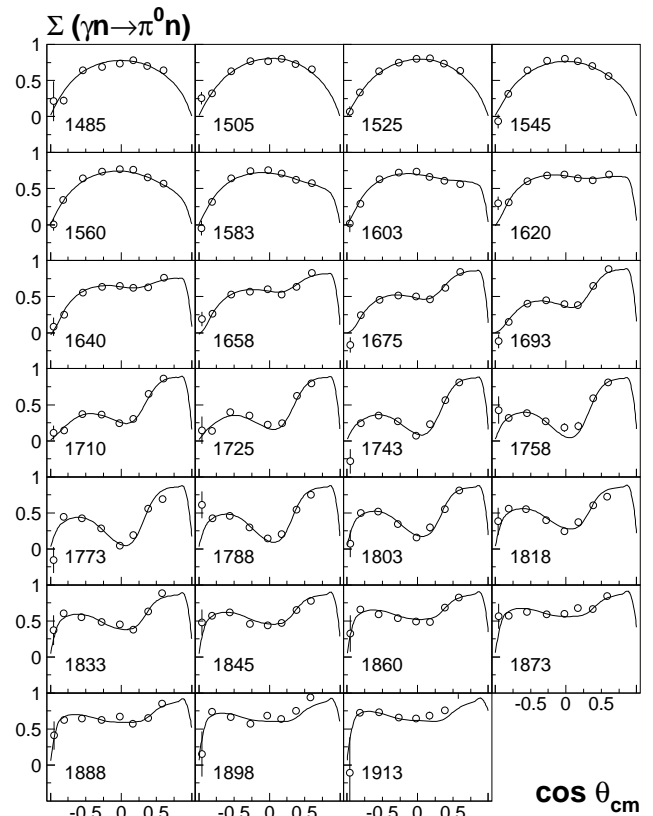


Fig. 8. Σ polarization for $\gamma n \rightarrow \pi^0 n$ [73].

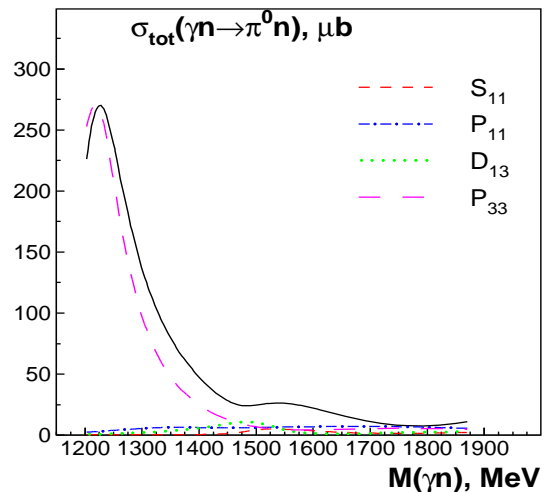


Fig. 9. Total cross section for $\gamma n \rightarrow \pi^0 n$.

4 The partial wave analysis

The fits are based on the BnGa partial wave analysis program. The program is documented in a series of papers [78, 79, 80, 81]. This paper is based on our latest solution BG2011-02 [27]. Here, we mention a few points which are of particular interest for this work.

In the fits, the partial waves (up to $J = 7/2$) were described in the framework of the K-matrix/P-vector approach, while the contribution of higher partial waves contribute only via Regge t and u -channel exchange ampli-

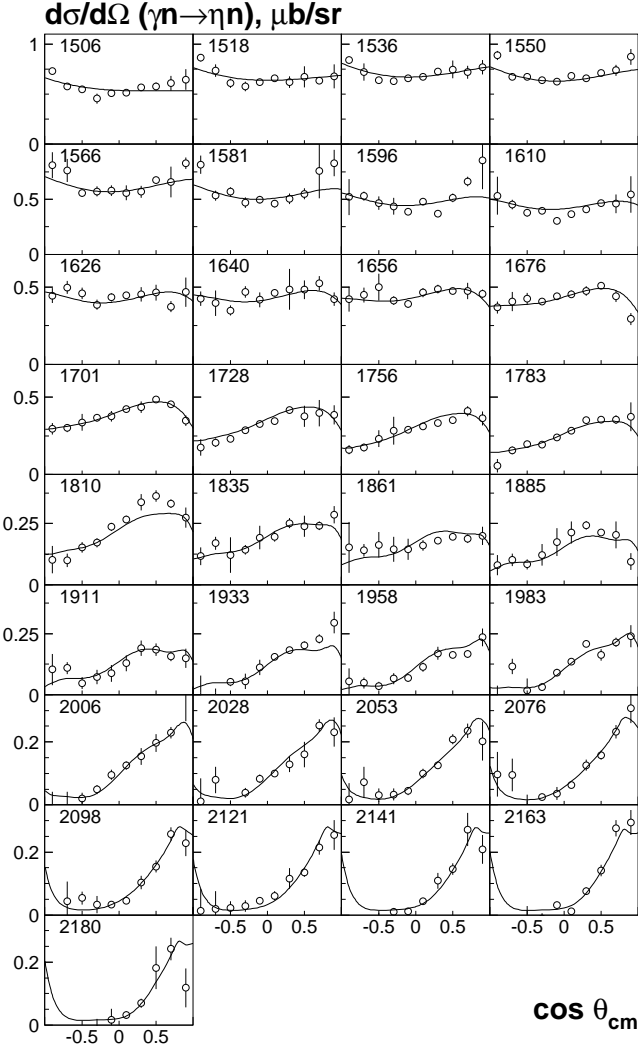


Fig. 10. Differential cross section for $\gamma n \rightarrow \eta n$ [74].

tudes. Thus, fixing all parameters related to the description of the pion and photo-induced reactions, we obtained a rather good description of the data listed in Table 1. The quality of the description obtained with the solution BG2011-02 is demonstrated in the fourth column of Table 1 and denoted as χ_0^2 .

The solution we found was not unique. Starting from different initial γn couplings for the nucleon resonances we observed several minima. In one case (like the one shown in Table 1), the differential cross section and beam asymmetry were well described while the fit to target and recoil asymmetry was only fair. In other fits the target and recoil asymmetries were described with a notably better χ^2 while differential cross section and beam asymmetry had a worse description providing almost same total χ^2 .

A refit of the full data base including pion and photo-induced reactions off protons with all parameters free improved very notably the description of the data on photo-production off neutrons while the fit to pion and photo-induced reactions using protons did not deteriorate no-

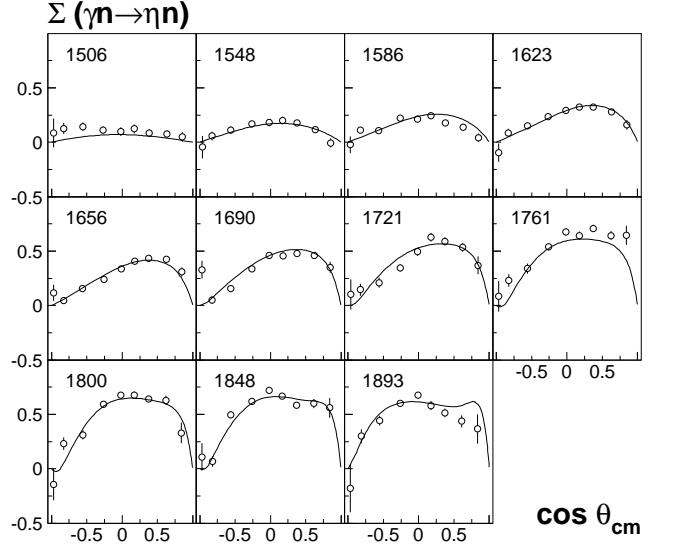


Fig. 11. Σ polarization for $\gamma n \rightarrow \eta n$ [75].

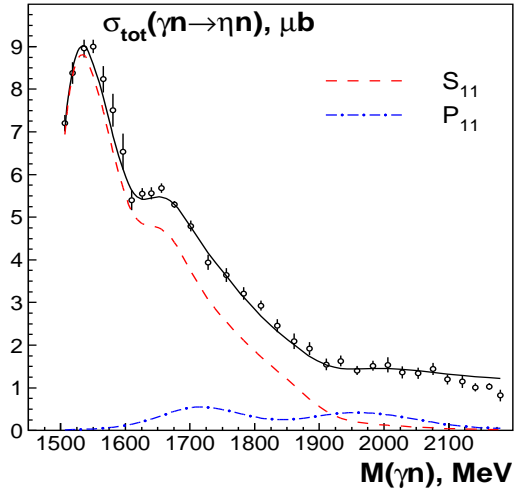


Fig. 12. Total cross section for $\gamma n \rightarrow \eta n$.

tably. The improvement of the description of the γn data can be estimated from the χ_f^2 given in the last column of Table 1.

However, also the full refit of all data did not lead to a unique solution: there is still a number of acceptable solutions with rather different γn couplings of the resonances in the third and fourth resonance region. Probably this is not a big surprise: most of these states have rather small couplings to the πN channel and cannot be reliably defined from the present data. As the result, in a number of solutions the fit returned for these states large γn amplitudes with destructively interfering couplings which provided a slightly better description than smaller and more realistic amplitudes. When these couplings were fixed to zero, the result was often only a small deterioration of the description. In the present analysis, all these solutions were used to estimate the systematic errors of the neutron helicity couplings. Obviously, γn couplings of high-mass resonances cannot yet be defined precisely; future data on photoproduction of open strangeness and of multi-meson

Table 2. The γn helicity couplings of nucleon states ($\text{GeV}^{-1/2}10^{-3}$) calculated as residues in the pole position and corresponding Breit-Wigner couplings. The sign of a helicity amplitude at the pole position is chosen to have a phase $< 180^\circ$. For convenience of the reader we give pole positions from [27] in last two columns.

	$\pm A_n^{1/2} $	Phase	$A_{n(BW)}^{1/2}$	$\pm A_n^{3/2} $	Phase	$A_{n(BW)}^{3/2}$	M_{pole}	$\frac{1}{2}\Gamma_{\text{pole}}$
$N(1535)1/2^-$	-103 ± 11	$8\pm 5^\circ$	-93 ± 11				1501 ± 4	134 ± 11
$N(1650)1/2^-$	25 ± 20	$0\pm 15^\circ$	25 ± 20				1647 ± 4	103 ± 8
$N(1895)1/2^-$	17 ± 10	$5\pm 30^\circ$	13 ± 6				1900 ± 15	90_{-15}^{+30}
$N(1440)1/2^+$	35 ± 12	$25\pm 25^\circ$	43 ± 12				1370 ± 4	190 ± 7
$N(1710)1/2^+$	-40 ± 20	$-30\pm 25^\circ$	-40 ± 20				1687 ± 17	200 ± 25
$N(1880)1/2^+$	-60 ± 50	$-30\pm 40^\circ$	-60 ± 50				1860 ± 35	270 ± 70
$N(1520)3/2^-$	-49 ± 8	$-3\pm 8^\circ$	-49 ± 8	-114 ± 12	$1\pm 3^\circ$	-113 ± 12	1507 ± 3	111 ± 5
$N(1700)3/2^-$	31 ± 10	$-50\pm 30^\circ$	25 ± 10	-35 ± 18	$-30\pm 30^\circ$	-32 ± 18	1770 ± 40	420 ± 180
$N(1875)3/2^-$	9 ± 6	not def.	10 ± 6	-19 ± 15	not def.	-20 ± 15	1860 ± 23	200 ± 20
$N(2120)3/2^-$	112 ± 40	$-30\pm 25^\circ$	110 ± 45	40 ± 30	$-55\pm 60^\circ$	40 ± 30	2110 ± 50	340 ± 45
$N(1720)3/2^+$	-80 ± 50	$-20\pm 30^\circ$	-80 ± 50	-140 ± 65	$5\pm 30^\circ$	-140 ± 65	1660 ± 30	450 ± 100
$N(1900)3/2^+$	-5 ± 35	$30\pm 30^\circ$	0 ± 30	-60 ± 40	$45\pm 40^\circ$	-60 ± 45	1900 ± 30	200_{-60}^{+100}
$N(1675)5/2^-$	-61 ± 7	$-10\pm 5^\circ$	-60 ± 7	-89 ± 10	$-17\pm 7^\circ$	-88 ± 10	1654 ± 4	151 ± 5
$N(2060)5/2^-$	27 ± 12	$-45\pm 25^\circ$	25 ± 11	-40 ± 18	$55\pm 30^\circ$	-37 ± 17	2040 ± 15	390 ± 25
$N(1680)5/2^+$	33 ± 6	$-12\pm 9^\circ$	34 ± 6	-44 ± 9	$8\pm 10^\circ$	44 ± 9	1676 ± 6	113 ± 4
$N(1860)5/2^+$	-20 ± 13	$50\pm 45^\circ$	21 ± 13	35 ± 17	$25\pm 35^\circ$	34 ± 17	1830_{-60}^{+120}	250_{-50}^{+150}
$N(2000)5/2^+$	-17 ± 12	$-50\pm 60^\circ$	-18 ± 12	-35 ± 20	$-50\pm 90^\circ$	-35 ± 20	2030 ± 110	480 ± 100
$N(1990)7/2^+$	-45 ± 20	$-50\pm 35^\circ$	-45 ± 20	-50 ± 25	$-45\pm 40^\circ$	-52 ± 27	2030 ± 65	260 ± 60
$N(2190)7/2^-$	-15 ± 12	$50\pm 40^\circ$	-15 ± 13	-33 ± 20	$25\pm 20^\circ$	-34 ± 22	2150 ± 25	330 ± 30

final states and data on double polarization will certainly improve the situation.

5 Results

The helicity couplings calculated from pole residues are given in Table 2 for all fitted resonances together with the Breit-Wigner couplings reconstructed following the prescription given in [27]. Due to the multitude of solutions with acceptable χ^2 , the results on neutron helicity amplitudes vary over some range. The spread of results is used to estimate the error bands in Table 2. The comparison of these couplings with results of other analyses is shown in Table 3. Several of our couplings differ rather notably from average values given in the review of Particle Data Group [85]. However, our results are often in a good agreement with the latest analysis of the γn data from the George Washington University group (SAID) [36].

As in our previous analysis of the γn data [33], we found a large γn coupling for $N(1535)1/2^-$. The coupling is larger than the value found in the SAID solutions SN11 [83] and GB12 [36], and very significantly larger compared to solution [34]. In the latest analysis of the γn data, the SAID group found an alternative solution GZ12 [36] which provides a slightly better description of the data and is

fully compatible with our result: see numbers in parenthesis in Table 3. We remark that the SQTm analysis [32] predicts a value $A_n^{1/2} = (-90 \pm 5)10^{-3}\text{GeV}^{-1/2}$ for this state, in excellent agreement with our results.

For the second $1/2^-$ state $N(1650)$, our fit optimized for a positive helicity coupling while most other analyses - our own previous result [33] and both recent SAID results [36,83] - report negative values. In the present fits, this coupling optimized always at a positive value. This result seems to be driven by the different interference effect in η photoproduction from γp and γn initial states: in $\gamma n \rightarrow n\eta$, a peak structure at 1680 MeV is observed in the $N\eta$ invariant mass which is absent in $\gamma p \rightarrow p\eta$. However, even in solutions where this peak structure was described as a contribution from $N(1680)1/2^+$, and some interference in the $1/2^-$ partial wave, the $N(1650)1/2^-$ helicity coupling became smaller but remained positive. To investigate systematically our result we started fits from our solutions reported in [33] and fitted with free parameters or fixed to zero the couplings of high mass states which were not included in the fit at that time. However, in all cases the present fits optimize for a positive coupling. This result was reproduced by both solutions BG2011-01 and BG2011-02.

Table 3. The comparison of our γn helicity couplings ($\text{GeV}^{-1/2}10^{-3}$) for Breit-Wigner resonances with SAID solution GB12 [82], solution SN11 [83], MAID solution [84], solution ShMa [88], PDG average numbers [85], and SQTm projections [32]. In the case of GB12 solution [82] the alternative solution for the $J^P = 1/2^-$ partial wave GZ12 is shown in parenthesis.

	$A_{n(BW)}^{1/2}$	$A_{(BW)}^{3/2}$		$A_{(BW)}^{1/2}$	$A_{(BW)}^{3/2}$
$N(1535)1/2^-$	-93±11		$N(1440)1/2^+$	43±12	
GB12	-58±6 (-85±15)		GB12	48±4	
SN11	-60±3		SN11	45±15	
MAID	-51		MAID	54	
ShMa	-49±3		ShMa	40±5	
PDG12	-46±27		PDG12	40±10	
SQT03	-90±6				
$N(1650)1/2^-$	25±20		$N(1710)1/2^+$	-40±20	
GB12	-40±10 (?±?)		GB12		
SN11	-26±8		SN11		
MAID	9		MAID		
ShMa	11±2		ShMa	17±3	
PDG12	-15±21		PDG12	2±14	
SQT03	-31±3				
$N(1520)3/2^-$	-49±8	-113±12	$N(1720)3/2^+$	-80±50	-140±65
GB12	-46±6	-115±5	GB12	ambiguous	ambiguous
SN11	-47±2	-125±2	SN11	-21±4	-38±7
MAID	-77	-154	MAID	-3	-31
ShMa	-38±3	-101±4	ShMa	-2±1	-1±2
PDG12	-59±9	-139±11	PDG12	4±15	-10±20
SQT03	-44±7	-140±5			
$N(1675)5/2^-$	-60±7	-88±10	$N(1680)5/2^+$	34±6	-44±9
GB12	-58±2	-80±5	GB12	26±4	-29±2
SN11	-42±2	-60±2	SN11	50±4	-47±2
MAID	-62	-84	MAID	28	-38
ShMa	-40±4	-68±4	ShMa	29±2	-59±2
PDG12	-43±12	-58±13	PDG12	29±10	-33±9
SQT03	-38±3	-53±8			

In our fits, the opposite signs of the $N(1650)1/2^-$ and $N(1535)1/2^-$ helicity amplitudes are required when the dip-bump structure in the $\gamma n \rightarrow n\eta$ total cross section in Fig. 12 is assigned to the $J^P = 1/2^-$ wave. If the two helicity amplitudes are forced to have the same sign, the peak-bump structure is described by $N(1710)1/2^+ \rightarrow n\eta$ decays. The description is improved when a narrow $N(1685)$ resonance [86,87] is admitted in the fit in addition to $N(1710)$, yet the overall χ^2 remains significantly worse than in the case where opposite signs of the $N(1650)1/2^-$ and $N(1535)1/2^-$ helicity amplitudes are admitted. Opposite signs for $N(1650)1/2^-$ and $N(1535)1/2^-$ helicity amplitudes are also found in the recent analysis by Shrestha

and Manley [88]. The MAID solution [84] is compatible with our value as well. The SAID group did not report the exact number for the GZ12 solution: only magnitude of the coupling was mentioned ($\approx 20 \text{ GeV}^{-1/2}10^{-3}$ [82]).

We mention that our old (now superseded) result was derived from an insufficient data base. A fit with a free helicity coupling for $N(1650)$ did not converge properly. Hence the direct coupling was set to zero. Through rescattering, a finite (negative) value for the $N(1650)$ helicity coupling emerged. Now, the data base has much improved, and we do no longer quote helicity amplitudes which led to a bad convergence property of the fit (except for error studies).

The γn coupling of the Roper resonance $N(1440)1/2^+$ was found to be in a good agreement with results of other analyses. The fit also optimized at a rather large γn couplings for the $N(1710)1/2^+$ and $N(1880)1/2^+$ states, the latter with very large uncertainties. However, there is a strong interference between these couplings: both states contribute very little to π and η photoproduction and therefore their couplings cannot be defined reliably from the analysis of the present data set. If the primary photo production coupling of both higher $1/2^+$ states are fixed to zero, the description does not change significantly. Even in this fit we found - via rescattering - rather large γn couplings as pole residues. All these solutions were included to define systematic errors for couplings given in Table 2.

Both $N(1520)3/2^-$ γn couplings were found to be notably smaller than the average PDG values while our present result is fully compatible with the latest fit of the SAID group; their values are thus confirmed by our analysis. We found rather small helicity couplings for $N(1875)3/2^-$: the fit does not demand a contribution from this resonances. Also the neutron helicity amplitudes for $N(1700)3/2^-$ are not well fixed by the data. The $A_n^{1/2}$ coupling of the $N(2120)3/2^-$ state was found to be rather large and stable in the fit. However in this energy range there are only good data in the photoproduction of charged pion [36]. Therefore a presence of a Δ state with $J^P = 3/2^-$ can change the situation significantly.

Our result for the helicity amplitudes of $N(1675)5/2^-$ is also rather different from the average PDG values but again coincides remarkably well with the latest SAID analysis GB12 and with MAID. The SQTm projections of -38 ± 5 and -53 ± 8 agree with PDG averages as well as with SN11 but are at variance with our result and GB12. We also believe that we have obtained reliable numbers for $N(2060)5/2^-$: in our solutions this state contributes to both η and π photoproduction reactions.

Our result for the $A_n^{3/2}$ helicity coupling of $N(1680)5/2^+$ deviates by more than one standard deviation from the SAID fit GB12, but is in a good agreement with the SN11 solution. Probably, there is some freedom in this region which should be fixed by future double polarization data. We found rather small couplings for the higher $5/2^+$ states. The large systematic errors here are not surprising: these couplings are difficult to define without including other final states like ΛK or $N\pi\pi$ and double polarization data.

The fits based on the solution BG2011-02 produced a notably better description of the data than fits based on the solution BG2011-01. Hence we provide the γn couplings for $N(1990)7/2^+$ obtained with the solution based on BG2011-02. Excluding these couplings from the fit leads to a deterioration of the description in the high mass region, hence we consider these results as reliable.

We have found a rather small improvement from the γn couplings of the $N(2190)7/2^-$ state, and the couplings were almost compatible with zero.

The size of the photocouplings of the $N(1720)3/2^+$ is a highly controversial topic. Already our analysis of γp interactions showed a large discrepancy between our result and the mean PDG value [85]. The discrepancy was partly

resolved by the latest SAID analysis [83] where the $A_p^{1/2}$ coupling was found to be compatible with our result. But our $A_p^{3/2}$ value is still more than three times larger than the SAID result. In our present analysis we found γn couplings which are also dramatically larger than those found in the SAID analysis SN11 [83]. In the analysis GB12-GZ12 the couplings for $N(1720)3/2^+$ are not given: the fit found a number of solutions with rather different contributions from this state.

One of the problems may be related to the complicated structure in this partial wave; a second problem is due to the possibility to assign intensity in the 1700 MeV region to $N(1720)3/2^+$, to $N(1710)1/2^+$ or to $N(1700)3/2^-/\Delta(1700)3/2^-$. A third source for the differences in the results for the $N(1720)3/2^+$ helicity amplitudes could be the difference of the methods used to extract resonance parameters. This state is rather broad and highly inelastic: the elasticity is about 10% only. The elastic pole residue has a very large phase: it varies between -90° and -140° . The phase reflects a large contribution from non-resonant terms which make it difficult to treat the state as Breit-Wigner resonance. The amplitude pole corresponding to this state is located in the 1660-1690 MeV region, and the dominant decay into the $2\pi p$ final state is complicated due to the opening of the $\pi N(1520)3/2^-$ channel (which was found to be rather strong in a number of our solutions). Further, this resonance is close to $\Delta(1600)3/2^+$, a resonance with parameters which are also not firmly defined. The presence of $N(1900)3/2^+$ and $N(1875)3/2^-$ makes the picture even more complicated. These uncertainties contribute to the large errors for the $N(1720)3/2^+$ helicity amplitudes.

6 Conclusion

Starting from solution BG2011-02, we obtained a rather good description of the π and η photoproduction data off neutrons which was improved further by allowing the fit to adjust slightly also masses, widths, coupling constants, and background terms in an overall fit which includes also data on photoproduction off protons and pion-induced reactions. The results for the helicity couplings for photoproduction off neutrons were presented and compared to results from other analyses.

The couplings of several 4-star resonances differ notably from average PDG values but are mostly in very good agreement with the latest SAID analysis GB12(GZ12) [36]. For the $N(1535)1/2^-$ state our coupling is fully compatible with one of the SAID solutions (GZ12). The $N(1650)1/2^-$ helicity amplitude differs from our previous result [33] and from results of the two SAID solutions SN11 and GZ12. The $N(1720)3/2^+$ helicity amplitudes are controversial (as they are in the case of proton helicity amplitudes). More data are required to resolve these ambiguities. We also have defined the γn helicity couplings for radial excitations in the third and fourth resonance region. However in most cases these numbers should be taken with care and may rather be considered as initial values for a

future analysis when new data with other final states will be included into the fit.

Acknowledgements

We would like to thank the members of SFB/TR16 for continuous encouragement. We acknowledge support from the Deutsche Forschungsgemeinschaft (DFG) within the SFB/TR16. V. Burkert acknowledges support from the US Department of Energy under contract DE-AC05-06OR23177.

References

1. A. J. G. Hey and R. L. Kelly, Phys. Rept. **96**, 71 (1983).
2. E. Klempt and J. M. Richard, Rev. Mod. Phys. **82**, 1095 (2010).
3. I. G. Aznauryan and V. D. Burkert, Prog. Part. Nucl. Phys. **67**, 1-54 (2012).
4. E. Klempt and A. Zaitsev, Phys. Rept. **454**, 1 (2007).
5. V. V. Anisovich *et al.*, "Mesons and baryons: Systematization and methods of analysis," *Hackensack, USA: World Scientific (2008) 580 p.*
6. J. F. Gunion and R. S. Willey, Phys. Rev. D **12**, 174 (1975).
7. S. Godfrey and N. Isgur, Phys. Rev. D **32**, 189 (1985).
8. M. Koll *et al.*, Eur. Phys. J. A **9**, 73 (2000).
9. R. Ricken *et al.*, Eur. Phys. J. A **9**, 221 (2000).
10. S. Capstick and N. Isgur, Phys. Rev. D **34**, 2809 (1986).
11. P. Stassart and F. Stancu, Z. Phys. A **359**, 321 (1997).
12. U. Löring, B. C. Metsch and H. R. Petry, Eur. Phys. J. A **10**, 395, 447 (2001).
13. M. Ferraris *et al.*, Phys. Lett. B **364**, 231 (1995).
14. L. Y. Glozman, W. Plessas, K. Varga and R. F. Wagenbrunn, Phys. Rev. D **58**, 094030 (1998).
15. N. Suzuki *et al.*, Phys. Rev. Lett. **104**, 042302 (2010).
16. R. G. Edwards *et al.*, Phys. Rev. D **84**, 074508 (2011).
17. R. G. Edwards *et al.*, "The Flavor Structure of the Excited Baryon Spectra from Lattice QCD," arXiv:1212.5236 [hep-ph].
18. S. Weinberg, Physica A **96**, 327 (1979).
19. V. Bernard, N. Kaiser and U. -G. Meißner, Int. J. Mod. Phys. E **4**, 193 (1995).
20. P. C. Bruns, M. Mai and U. G. Meißner, Phys. Lett. B **697**, 254 (2011).
21. M. Mai, P. C. Bruns and U. -G. Meißner, Phys. Rev. D **86**, 094033 (2012).
22. M. F. M. Lutz, G. Wolf and B. Friman, Nucl. Phys. A **706**, 431 (2002) [Erratum-ibid. A **765**, 431 (2006)].
23. G. Höhler *et al.*, "Handbook Of Pion Nucleon Scattering," Fachinform. Zentr. Karlsruhe 1979, 440 P. (Physics Data, No.12-1 (1979)).
24. R. E. Cutkosky *et al.*, "Pion - Nucleon Partial Wave Analysis," 4th Int. Conf. on Baryon Resonances, Toronto, Canada, Jul 14-16, 1980. Published in Baryon 1980:19 (QCD161:C45:1980).
25. R. A. Arndt *et al.*, Phys. Rev. C **74**, 045205 (2006).
26. V. D. Burkert, EPJ Web Conf. **37**, 01017 (2012).
27. A. V. Anisovich *et al.*, Eur. Phys. J. A **48**, 15 (2012).
28. S. Capstick and W. Roberts, Prog. Part. Nucl. Phys. **45**, S241 (2000).
29. T. Gutsche *et al.*, "Nucleon resonances in AdS/QCD," arXiv:1212.6252 [hep-ph].
30. A. J. G. Hey and J. Weyers, Phys. Lett. B **48**, 69 (1974).
31. W. N. Cottingham and I. H. Dunbar, Z. Phys. C **2**, 41 (1979).
32. V. D. Burkert *et al.*, Phys. Rev. C **67**, 033204 (2003).
33. A. V. Anisovich *et al.*, Eur. Phys. J. A **41**, 13 (2009).
34. R. A. Arndt, I. I. Strakovsky and R. L. Workman, Phys. Rev. C **53**, 430 (1996).
35. W. Chen *et al.*, Phys. Rev. Lett. **103**, 012301 (2009).
36. W. Chen *et al.*, Phys. Rev. C **86**, 015206 (2012).
37. P. E. Argan *et al.*, Nucl. Phys. A **296**, 373 (1978).
38. M. Beneventano *et al.*, Nuovo Cim. A **19**, 529 (1974).
39. T. Fujii *et al.*, Nucl. Phys. B **120**, 395 (1977).
40. G. von Holtey *et al.*, Nucl. Phys. B **70**, 379 (1974).
41. G. Neugebauer *et al.*, Phys. Rev. **119**, 1726 (1960).
42. P. E. Scheffler and P. L. Walden, Nucl. Phys. B **75**, 125 (1974).
43. P. Benzet *et al.*, Nucl. Phys. B **65**, 158 (1973).
44. V. Rossiet *et al.*, Nuovo Cim. A **13**, 59 (1973).
45. F. V. Adamian *et al.*, J. Phys. G **15**, 1797 (1989).
46. J. Alspectoret *et al.*, Phys. Rev. Lett. **28**, 1403 (1972).
47. G. Knieset *et al.*, Phys. Rev. D **10**, 2778 (1974).
48. K. Kondoet *et al.*, Phys. Rev. D **9**, 529 (1974).
49. G. Mandaglioet *et al.*, Phys. Rev. C **82**, 045209 (2010).
50. L. O. Abrahamian, Sov. J. Nucl. Phys. **32**, 69 (1980).
51. V. B. Ganenko, Sov. J. Nucl. Phys. **23**, 511 (1976).
52. F.F.Liu *et al.*, Phys. Rev. B **136**, 1183 (1964).
53. A. M. Sandorfi, 7th International Conference on the Structure of Baryons, Oct 3-7 (1995), Santa Fe, New Mexico.
54. V. L. Agranovich *et al.*, VANT **8**, 5 (1989).
55. K. H. Althoff *et al.*, Nucl. Phys. B **96**, 497 (1975).
56. K. H. Althoff *et al.*, Nucl. Phys. B **116**, 253 (1976).
57. K. Fujii *et al.*, Nucl. Phys. B **187**, 53 (1981).
58. H. Takeda *et al.*, Nucl. Phys. B **168**, 17 (1980).
59. J. P. Kenemuth, P.C.Stein, Phys. Rev. **129**, 2259 (1963).
60. R. Bagheriet *et al.*, Phys. Rev. C **38**, 875 (1988).
61. J. C. Comiso *et al.*, Phys. Rev. D **12**, 719 (1975).
62. G. J. Kimet *et al.*, Phys. Rev. D **40**, 244 (1989).
63. A. Shafiet *et al.*, Phys. Rev. C **70**, 035204 (2004).
64. M. T. Tran *et al.*, Nucl. Phys. A **324**, 301 (1979).
65. Wang, Ph.D Thesis 1992, see [77].
66. A. L. Weiss *et al.*, Nucl. Phys. B **101**, 1 (1975).
67. J. C. Stasko *et al.*, Phys. Rev. Lett. **72**, 973 (1994).
68. G. J. Kimet *et al.*, Phys. Rev. D **43**, 687 (1991).
69. A. Ando *et al.*, "Physik Daten, Physics Data," Fach-Informationszentrum, Karlsruhe, 1977.
70. C. Bacciet *et al.*, Phys. Lett. C **39**, 559 (1972).
71. Y. Hemmi *et al.*, Nucl. Phys. B **55**, 333 (1973).
72. Klimesmith, Ph.D Thesis 1967, see [77].
73. R. Di Salvo *et al.*, Eur. Phys. J. A **42**, 151 (2009).
74. I. Jaegle *et al.*, Phys. Rev. Lett. **100**, 252002 (2008).
75. A. Fantini *et al.*, Phys. Rev. C **78**, 015203 (2008).
76. V. E. Tarasov *et al.*, Phys. Rev. C **84**, 035203 (2011).
77. W.J. Briscoe *et al.*, CNS Data Analysis Center, GWU, <http://gwdac.phys.gwu.edu/>
78. A. Anisovich, E. Klempt, E. Sarantsev, U. Thoma, Eur. Phys. J. A **24**, 111-128 (2005).
79. A. V. Anisovich, A. V. Sarantsev, Eur. Phys. J. A **30**, 427-441 (2006).
80. E. Klempt, A. V. Anisovich, V. A. Nikonov, A. V. Sarantsev and U. Thoma, Eur. Phys. J. A **29**, 307 (2006).

81. A. V. Anisovich *et al.*, Eur. Phys. J. A **34**, 129 (2007).
82. R. L. Workman, M. W. Paris, W. J. Briscoe and I. I. Strakovsky, Phys. Rev. C **86**, 015202 (2012).
83. R. L. Workman, W. J. Briscoe, M. W. Paris and I. I. Strakovsky, Phys. Rev. C **85**, 025201 (2012).
84. D. Drechsel, S. S. Kamalov and L. Tiator, Eur. Phys. J. A **34**, 69 (2007).
85. J. Beringer *et al.*, Phys. Rev. D **86**, 010001 (2012).
86. V. Kuznetsov *et al.*, Phys. Rev. C **83**, 022201 (2011).
87. I. Jaegle R. Beck *et al.*, Eur. Phys. J. A **47**, 89 (2011).
88. M. Shrestha and D. M. Manley, Phys. Rev. C **86**, 055203 (2012).

